Science & Technology Facilities Council

Technical Report

On accurate and time efficient solution of primal-mixed finite-element equations in multiscale solid mechanics

Iain S. Duff and Dubravka Mijuca

July 23, 2009

RAL-TR-2009-013

Library and Information Services
SFTC Rutherford Appleton Laboratory
Harwell Science and Innovation Campus
Didcot
OX11 0QX
UK
Tel: +44 (0)1235 445384
Fax: +44(0)1235 446403
Email: library@rl.ac.uk

ISSN 1358-6254

RAL-TR-2009-013

On accurate and time efficient solution of primal-mixed finite element equations in multiscale solid mechanics[1]

Iain S. Duff[2] and Dubravka Mijuca[3]

ABSTRACT

In order to identify the best technique to solve a class of geometrically multiscale model problems in thermoelasticity, we examine a combination of a primal–mixed finite element approach and direct sparse solvers and matrix scaling routines. The criteria for optimality are robustness, accuracy and execution time. It will be shown that the present finite element approach, where displacement and stress variables are simultaneously solved from large scale indefinite poorly scaled systems of equations using the sparse *HSL* solver `MA57` with the aid of the matrix scaling routines `MC64` or `MC30` during the factorization process, enables a reliable solution even if hexahedral finite elements in a mesh differ in size up to six orders of magnitude. A number of tests in multiscale elasticity and thermoelasticity are examined to test the accuracy and execution time efficiency of the proposed solution approach on a standard PC computing platform.

Keywords:: solid mechanics, thermoelasticity, geometrically multiscale, primal–mixed finite element, reliable, sparse, indefinite, time efficient, scaling, HSL, multifrontal method.

AMS(MOS) subject classifications:: 65F05, 65F10, 65F50, 65G50.

---

[1]Current reports available by anonymous ftp to `ftp.numerical.rl.ac.uk` in directory pub/reports. This report is in file dumiRAL2009013.pdf. The report also available through the URL `www.numerical.rl.ac.uk/reports/reports.html`. It is also available as the CERFACS Technical Report TR/PA/09/67.

[2]email: iain.duff@stfc.ac.uk. The work of this author was supported by the EPSRC Grants EP/E053351/1 and EP/F006535/1.

[3]email: dmijuca@fgm.edu.yu. Faculty of Civil Construction Management, University UNION, Cara Dusana 62–64, 11000 Belgrade, Serbia. The work of this author was supported by the Ministry of Science of Republic of Serbia Grant 144007.

Computational Science and Engineering Department
Atlas Centre
Rutherford Appleton Laboratory
Oxon OX11 0QX

July 23, 2009

Contents

1. Introduction 1
2. Field problems 2
3. Finite element configurations 4
4. System matrix properties 5
5. *HSL*, formerly the Harwell Subroutine Library 6
5.1. *HSL* solution routines 6
5.2. *HSL* matrix scaling routines 7
5.3. *HSL* matrix ordering routines 7
5.4. Error estimates 7
6. Examples 7
6.1. Bending of the clamped plate 8
6.2. Long steel coated shaft loaded by the uniform traction 10
6.3. Long steel coated shaft loaded by the prescribed temperature 11
6.4. Nanoindentation. One–to–one bridging with molecular dynamic simulation. 12
6.5. Composite material with embedded fibre optic sensor 14
7. Conclusion 16
Acknowledgements 16
References 17

1. Introduction

Although the finite element method [1, 2] has been heavily used by the engineering community for more than five decades, there is still the need for a fully three–dimensional, stable, accurate [3, 4] and time–efficient approach to multiscale multimaterial solid mechanics. Nowadays, accurate and reliable prediction of the state of stress and defect structure over subregions with different geometric scales and material interfaces in thermo-mechanically loaded structures are a top priority in a number of industries. For example, there are new demands for the accurate determination of interfacial stresses in coated structural components for thermal protection or in layered composite structures in which residual stresses might arise during manufacturing processes. Similar complexity is found in sandwich structures with nearly incompressible foam in their core. This is also the case in drilling devices for oil, which have an extremely high ratio of minimal and maximal axial dimensions. Furthermore, in determining the stresses in embedded fibre optic sensors for nondestructive testing, or in the analysis of filling techniques of cavity walls of the restored tooth in order to reduce polymerization shrinkage stresses. All abovementioned examples are in their nature multiscale [7, 8], and demand a full three-dimensional insight from the simulation process. Indeed, a fully three–dimensional approximation of model problem geometry without dimensional reduction [9] helps to analyse material behaviour through its thickness and geometrical scales and enables possible bridging with micromechanical [10] and particle [18] simulation approaches.

It is generally recognized that heavily used displacement–based finite element methods (primal finite element approaches) are not robust in situations where material is (almost) incompressible, in the inelastic behaviour of many materials, and also in the analysis of plates and shells, that is in an analysis of model problems which have much smaller thickness than the other two dimensions. For example, finite elements based on pure displacement interpolations are accurate in membrane-dominated situations but "lock" if bending is encountered [4]. In these situations the resulting finite element system matrix becomes too ill-conditioned to obtain an accurate solution [6]. In addition, the use of hexahedral finite elements to analyse thin solid bodies is not permitted due to the aspect ratio restriction. This is a major obstacle to using this approach in multiscale analysis, where the atomistic region is extended to the continuum region and therefore very narrow finite elements should be used in order to maintain a reasonable number of finite elements given the limitation in computer memory. On the other hand, idealization of the geometry by dimensional reduction [9] and detailed suppression techniques in order to reduce the complexity of the model is the major factor limiting the wider application of the finite element method where the material should be respected throughout its geometric scales. In addition, in primal approaches, the dual variable (heat flux, stress) is obtained *a posteriori*, which entails a loss of accuracy [1, 11, 12]. Therefore, for some analyses, other finite element approaches, such as mixed methods where more than one variable of interest is a solution variable (e.g. displacement and stress), need to be employed.

Therefore, in the present paper, we consider a reliable mixed HC$\boldsymbol{u/t}$ finite-element approach that has both primal and dual variables as solution variables (see Section 3) from the C^0 continuous subspace of the approximation functions (see [13, 14, 15]). This

enables the direct introduction of residual stresses and/or initial deformations directly without loss of accuracy due to numerical integration. The same approximation paradigm in transient heat transfer is presented in [14, 15]). Nevertheless, the time for execution of the present approach has not been examined before, although this is extremely important if it is to be used in transient or material nonlinear analysis, or in a real time engineering simulation.

From the mathematical point of view, the solution of these problems are sought as the critical points of saddle-point problems. Therefore, both resulting system matrices, for thermal and mechanical field problems, are indefinite. This is different from the primal finite element approach where the solution is sought using an extremal principle, and the resulting system matrix is positive definite. Therefore, one of the principal differences between these two finite–element approaches lies in the definiteness of their system matrices and the number of unknowns. It is obvious that a mixed approach results in more equations than a primal approach for the same model problem. This was considered as a serious drawback because it was thought that for the same accuracy the solution time would be increased. Nevertheless, it was shown in [20] that the present approach is faster than the classical raw primal displacement based finite element method, for the same accuracy per stress. It should be noted that all the finite element system matrices we are considering are sparse and symmetric. The present approach is straightforward. No stabilization techniques are required. The thermal and mechanical field problems are currently semi–coupled.

Nevertheless, multiscale model problems, where scale resolution of the model problems exceeds three orders of magnitude, were not examined in the abovementioned papers [13, 14, 15]. Novel tests on these cases, together with a detailed investigation of execution time efficiency and a recommendation for the most efficient solution technique will be the essential contribution of the present investigation.

It will be shown that the present approach is efficient in time and storage if it is used in combination with the sparse solvers `MA47` [21] or `MA57` [22] and matrix scaling routines `MC64` or `MC30`. They will be discussed in more detail in Section 5. It will be shown that these solvers are at least two orders of magnitude faster than a previously used in–house solver based on simple Gaussian elimination. Additionally, it is shown that scaling the system matrix prior to the factorization improves the accuracy and execution time of finite element equations and allows the solution of systems of equations with many more degrees of freedom [23].

It is hoped that practitioners as well as researchers in this field who are looking for guidance in the choice of a solution method for their own application will find this paper helpful.

2. Field problems

In the present paper we study a thermal stress problem in solid mechanics [24] that consists in determining the response of a body in terms of displacement $\mathbf{u}$ and stress $\mathbf{t}$, due to thermal and mechanical loading. In the case of traditional materials, where there is no heat production due to the strain rate, the thermal and stress analyses are semi–coupled

via thermal strains only. Thus, the governing equations of two separate field problems, transient heat transfer and mechanical, are semi–coupled via thermal strains calculated from the temperature field determined in the thermal analysis. In current work, thermal strains are considered as initial conditions for (mechanical) stress analysis and constitute only a datum for subsequent stress analysis [15, 25]. Otherwise, thermal and stress analyses are fully coupled.

The current primal–mixed finite-element approaches in non–multiscale elastostatics (HC$\mathbf{u}/\mathbf{t}$), and in transient heat (HC$T/\mathbf{q}$), were introduced in [13] and [15], respectively. It is proved that that these approaches are also reliable in the sense introduced on page 477 of [5], and are thus not sensitive to locking (see [4]). Let us briefly recall that the finite-element equation of the present elastostatic approach is given by:

$$\begin{pmatrix} X_{vv} & -Y_{vv} \\ -Y_{vv}^T & 0 \end{pmatrix} \begin{pmatrix} \boldsymbol{t}_v \\ \boldsymbol{u}_v \end{pmatrix} = \begin{pmatrix} -X_{vp} & Y_{vp} \\ Y_{vp}^T & 0 \end{pmatrix} \begin{pmatrix} \boldsymbol{t}_p \\ \boldsymbol{u}_p \end{pmatrix} - \begin{pmatrix} 0 \\ \boldsymbol{f}_p + \boldsymbol{p}_p \end{pmatrix}, \tag{2.1}$$

where submatrices of the system matrices in (2.1) are given by:

$$\begin{aligned} X_{\Lambda uv\Gamma st} &= \sum_e \int_{\Omega_i} \Omega_\Lambda^N S_N g^a_{(\Lambda)u} g^b_{(\Lambda)v} A_{abcd} g^c_{(\Gamma)s} g^d_{(\Gamma)t} T_L \Omega_\Gamma^L d\Omega \\ Y^{\Gamma q}_{\Lambda uv} &= \sum_e \int_{\Omega_?} \Omega_\Lambda^N S_N U_a^K \Omega_K^\Gamma g^a_{(\Lambda)u} \, g^{(\Gamma)q}_{(\Lambda)v} d\Omega \\ f^{\Lambda q} &= \sum_e \int_{\Omega_?} g_a^{(\Lambda)q} \Omega_M^\Lambda V^M f^a d\Omega \\ p^{\Lambda q} &= \sum_e \int_{\partial\Omega_{it}} g_a^{(\Lambda)q} \Omega_M^\Lambda V^M p^a d\partial\Omega \end{aligned} \tag{2.2}$$

The above expressions should be evaluated for each free degree of freedom (dof) connected to the pair of global nodes Λ and/or Γ of the finite element mesh, where Ω_L^Λ is the connectivity operator, which maps the set of global nodes Λ into the set of local nodes L defined on each element, and vice versa. X is an operator connecting the fourth order compliance tensor with the stress tensor, which is essentially the expression for the *complementary work* done by the system. Furthermore, Y connects the gradient of the displacement vector with the second order stress tensor. More, S and T, and U and V denote trial and test finite element basis interpolation functions for approximations of displacement and stress fields, respectively. That is, we use the same interpolation functions for each global node of the finite element mesh for the approximation of the stress and the displacement components. The more detailed description of matrix entries in (2.1) can be found in [13].

The system matrix in (2.1) is indefinite sparse and symmetric. The sparsity comes from intrinsic properties of finite element approximation functions which have local support only. The storage requirements can be reduced by storing only the upper triangle of the matrix because it is symmetric. The storage requirements are further reduced by storing only the entries which are nonzero. The pattern of the matrix and the number of entries are direct functions of the type of finite elements used for the mesh discretization of the

model problem and the FE node ordering routine. Elements with more nodes per finite element give rise to denser matrices.

The formulation given by (2.1) is a saddle-point problem, where the system matrix is of the 2×2 block form:

$$\begin{pmatrix} A & B^T \\ B & 0 \end{pmatrix} \tag{2.3}$$

where the block entry A is positive definite (see [13] and [15]).

We investigate for the first time in this paper the solution of the above system of linear finite element equations in geometrically multiscale thermoelasticity using the direct sparse solver `MA57` [22] and matrix scaling routines `MC30` [31] and `MC64` [32]. It will be shown that, without scaling the system matrix in equation (2.1) prior to the factorization, the solution fails. That is, for multiscale model problems in which finite elements significantly differ in size, over three or four orders of magnitude, the scaling of the system matrix enables the solution.

3. Finite element configurations

The topology of the present hexahedral continuous finite-element family HC$\boldsymbol{u}/\boldsymbol{t}$, for the approximation of displacement ($\boldsymbol{u}$) and stress ($\boldsymbol{t}$) field variables, is shown in Figure 3.1. In order to increase stability, the finite element subspaces for the approximation of dual variable are enriched by additional hierarchical shape functions. Therefore, finite elements contain 8 or 20 local nodes for the approximation of the displacement (primal variable), and 9 to 27 local nodes for the approximation of stress (dual variable). For example, the finite element configuration $HC8/9$ refers to the case where the primal variable is approximated by 8 local FE nodes and the dual variables are approximated by 9 local FE nodes. The same notation holds for other configurations examined in the present paper.

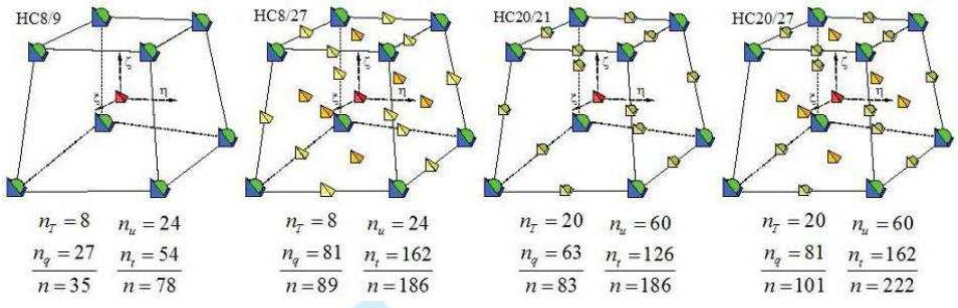

Figure 3.1. Finite element family HC

On the other hand, if there are 20 local nodes for the primal variable, then additional approximation functions (for nodes $9 - 20$) are quadratic in order to avoid the tessellation of curved boundaries. In this case the finite–element configurations that we consider are denoted by HC20/21 or HC20/27. As in the previous case, the approximation for the additional six FE nodes for the dual variables is performed by *hierarchical* shape functions in order to increase stability.

Let us emphasize that one finite element is reliable if it satisfies convergence requirements [5]. The convergence requirements for shape functions of an isoparametric element can be grouped into three categories, that is: completeness, compatibility and stability [1, 4]. If it satisfies completeness and compatibility, it is said to be consistent. It is also said that consistency and stability imply convergence. If the stability condition is satisfied, there will be no non-physical zero-energy modes (kinematic modes).

Therefore, the overall stability of mixed formulations based on the Hellinger–Reissner's principle that we use is guaranteed if two necessary conditions for stability are fulfilled: the first stability condition represented by ellipticity on the kernel condition, and the second stability condition represented by the so-called inf–sup condition. The satisfaction of the inf-sup condition ensures solvability and optimality of the finite-element solution, and it is very important that it is satisfied if the finite-element approach is to be used for the simulation of model problems under complex geometry, loading and material. It is dependent on the number of finite elements in the mesh (mesh size).

It was shown in [13] and [16] that the finite element HC8/27 is reliable in non-multiscale and multiscale analysis, respectively. There are many effective finite elements from the known literature that satisfy consistency, ellipticity and the inf–sup test, for example the MITC plate and shell bending finite elements [4]. Nevertheless, the FE element HC8/27 that we use here is the first where C^0 discretization is used for the approximation of the stress field without difficulty in the numerical solution of the linear system of equations [17].

4. System matrix properties

We consider a system matrix in (2.1) noting that, in the worst case, there is a maximum of 595 nonzero entries in each row, regardless of the number of finite element equations (degrees of freedom). Therefore, the system matrix is sparse, symmetric and indefinite [26]. The coefficients of that matrix are real and, furthermore, the upper left block X is positive definite. The crucial difficulty in solving this saddle-point problem comes from the indefiniteness of the system matrix. In addition, the system matrix is far from being banded so some classical solution procedures are inappropriate. An additional reordering must therefore be performed to limit the amount of fill–in and operations. It should be emphasized that the term *entry* is presently used to denote a nonzero matrix coefficient [27].

Leading concepts in the development of efficient solution algorithms that take advantage of the presence of many zeros are to store and operate only with *entries*. During the elimination process, the crucial requirement is to maintain sparsity in the factors in order to minimize the storage and work required for factorization. It is also important to pay great attention to the numerical stability of the factorization.

If a dense matrix is considered, requirements for the storage and solution times depend on the order n of the matrix and are $\mathcal{O}(n^2)$ and $\mathcal{O}(n^3)$, respectively. In the case of sparse matrix, a more reliable parameter for controlling the work and storage is the number of entries τ. It is the goal of sparse algorithms is to perform the computation in time and storage proportional to $O(n) + O(\tau)$ and although this is often not realized, sparse

algorithms are at worst asymptotically quadratic in n and so have much lower complexity than in the dense case.

Let us emphasize that the finite element software package *Straus7* [28] that we were using as a mesh generator, handles only the primal finite element method. It creates finite elements which have nodes only for displacement. This means that it reorders only eight or twenty nodes for the primal variable (hexahedral finite elements H8 and H20, with 8 or 20 primal nodes, respectively). Consequently, hierarchical nodes for dual variables which are added later in the present in–house code *FEMIX* [13] are placed at the end of the assembled matrix.

5. *HSL*, formerly the Harwell Subroutine Library

5.1. ***HSL* solution routines.** In this paper, we examine the execution time and storage requirements for the `MA57` [22] solver from *HSL* [29] that was developed for the direct solution of large sparse indefinite linear systems of equations. `MA57` is a sparse symmetric linear solver using a multifrontal approach with a choice of ordering schemes. It solves both positive definite and indefinite systems of equations. It has a range of options including several sparsity orderings, multiple right-hand sides, partial solutions, error analysis, scaling, a matrix modification facility, a stop and restart facility, and an option to determine the rank of highly deficient matrices. Although the default settings should work well in general, there are several parameters available to enable the user to tune the code for his or her problem class or computer architecture.

Like most sparse direct solvers, the algorithms are organized in three distinct computational phases: analyse, factorize and solve. The analyse phase is sometimes referred to as the symbolic factorization or ordering step. It preprocesses the system of equations and determines a pivotal sequence. It is often based purely on matrix structure. Furthermore, during the factorization phase, this sequence is used to compute the matrix factors. Finally, forward elimination followed by back substitution is performed during the solve phase using the stored factors. The factorization is usually the most time–consuming phase of the computation [30]. It should be emphasized that pivoting must be performed in the case of indefinite systems in order to increase stability and as well as for sparsity reasons.

It should be noted that *HSL* routines can also be used for the solution of linear systems of equations arising in primal finite element analysis, where the system matrix is positive definite. It can be a good alternative to iterative solution procedures. For further information about *HSL* routines, including licensing, the reader is referred to [29].

All the codes presently used for solving sparse equations and for scaling matrices (`MA` and `MC` codes) have been developed for inclusion in the mathematical software library HSL. Although all use of HSL requires a licence, individual HSL packages (together with their dependencies and accompanying documentation) are available without charge to individual academic users for their personal (non-commercial) research and for teaching; licences for other uses involve a fee. Details of the packages and how to obtain a licence plus conditions of use are available at http://www.cse.scitech.ac.uk/nag/hsl/hsl.shtml.

5.2. ***HSL* matrix scaling routines.** If an indefinite matrix is poorly scaled, it may be difficult to assess the accuracy of the solution. Scaling improves the robustness of the factorization [23]. Two scaling routines, `MC30` [31] and `MC64` [32], are considered in conjunction with the code `MA57`. These routines have quite different goals. `MC30` scales the matrix to make all entries close to one, while `MC64` permutes and scales the matrix so that the permuted matrix has each diagonal entry equal to one and all off-diagonal entries less than or equal to one in modulus. We present results obtained using the `MA57` equation solver, with and without scaling of the system matrix.

5.3. ***HSL* matrix ordering routines.** The choice of ordering scheme for reordering the entries in the sparse system matrix can be quite crucial to the performance of the equation solver. The `MA57` package has several different ordering schemes viz: MC47 [33] (including an option for efficiently handling dense rows [36]), `MA27H` [34], and METIS [35] which can be invoked in the analysis phase. The first two routines are *HSL* ordering routines, while the third is from a well known graph partitioning package and is based on a nested dissection ordering. MC47 provides an ordering for a sparse symmetric pattern matrix that is based on the approximate minimum-degree ordering algorithm (AMD). There is now an option in MC47 that takes special action if there are dense or nearly dense rows in the matrix [36].

5.4. **Error estimates.** Let us briefly recall how to calculate an estimate of the sparse backward error using the theory and measure developed by Arioli, Demmel, and Duff [37]. We use the notation $\bar{\mathbf{x}}$ for the computed solution and a modulus sign on a vector or matrix to indicate the vector or matrix obtained by replacing each entry by its modulus. The scaled residual

$$\frac{|\mathbf{b} - \mathbf{A}\bar{\mathbf{x}}|_i}{(|\mathbf{b}| + |\mathbf{A}||\bar{\mathbf{x}}|)_i} \tag{5.4}$$

is calculated for all equations except those for which the numerator is nonzero and the denominator is small. For the exceptional equations,

$$\frac{|\mathbf{b} - \mathbf{A}\bar{\mathbf{x}}|_i}{(|\mathbf{A}||\bar{\mathbf{x}}|)_i + ||\mathbf{A}_i||_\infty ||\bar{\mathbf{x}}||_\infty} \tag{5.5}$$

is used instead, where A_i is row i of A. Equations (5.4) and (5.5) represent the backward error and if their values are small then we have solved a system that is a small perturbation of the original system. If the residuals (5.4) and (5.5) are not sufficiently small, then the solver is regarded as having failed to solve the problem correctly. In the results which follow we use the quantity $\frac{\|\mathbf{b}-\mathbf{A}\bar{\mathbf{x}}\|}{\|\mathbf{b}\|+\|\mathbf{A}\|\|\bar{\mathbf{x}}\|}$ to measure the backward error.

6. Examples

In the present section, several model problems from elastostatics, under mechanical and/or thermal loads, are used to identify the best *HSL* sparse solver routine. The metric by which we judge "best" includes the execution time, that is the CPU times required to perform the analyse, factorize, and solve phases; the storage requirements, both total memory required and the number of nonzero entries (NE) in the matrix factor; and the

backward error. In earlier experiments we studied the influence of the value of the threshold parameter u but, as the solution time and accuracy was not very sensitive to this parameter, we use the default value of 0.01 for our runs in this paper. We had also earlier experimented with `MA47` [15] but as we have found `MA57` to be consistently better we now run tests for these metrics on only the combinations: `MA57`, `MA57`+`MC30`, and `MA57`+`MC64`. The performance with respect to scaling is highlighted.

It should be noted that the motive for the use of *HSL* solver routines was explained in [15], where it was shown that the `MA57`+`MC30` procedure [21] used for the solution of the mixed finite element equation system in heat transfer is two orders of magnitude faster than an in–house sparse Gaussian elimination solver.

All CPU times are in seconds. In all experiments, double precision (64-bit) reals were used. Numerical experiments were conducted on a PC Pentium(R) D CPU 2.8 GHz with 3.25GB of RAM with Physical Address Extension running under the operating system Microsoft Windows XP Professional Version 2002 Service Pack 2.

6.1. **Bending of the clamped plate.** The first problem that we consider is a classical elasticity problem of a clamped plate subjected to external uniform pressure $p = 100$. We model it as a three-dimensional structure so that we can trace the stress state along the thickness, and can bridge it with the full simulation on the micro or atomistic level in some regions in order to look for material damage or dislocation lines in a natural way. It is known that a primal finite element approach in conjunction with dimensional reduction suffers greatly from locking [5]. It is especially evident when the thickness decreases compared to the other axial dimensions, or when the material tends to become incompressible (plastification followed by fire). We show how it is easily solved using the mixed approach combined with scaling and efficient direct solvers. The extra complexity of this problem comes from the type of mechanical loading which contributes to the domination of the bending stresses over the membrane stresses.

The edge is of length $a = 2$, the thickness of the plate is $t = 0.01$, Young's modulus is $E = 1.7472 \cdot 10^7$, and Poisson's ratio is $\upsilon = 0.3$. The analytical solution for the maximal deflection at the plate centre C, calculated by Kirchhoff's plate theory, is w=1.26 [13]. Only a quarter of the plate is analysed due to the symmetry. The essential stress boundary conditions $t^{zz}|_{z=0.01} = -100$ are prescribed for the nodes lying on the upper surface of the plate. Clamped edges were simulated by zeroing degrees of freedom connected to the displacement ($u_x = u_y = u_z$) and transverse shear stress components ($t^{xz} = t^{yz}$). The model is discretized by a sequence of meshes with two layers of solid brick finite elements per thickness, that is $NEL \times NEL \times 2$, where NEL is 4, 8 or 16. Consequently, the axial dimension of the finite elements in the direction normal to the middle of the plate plane is $t/2 = 0.005$.

The solution times of `MA57`, using `MC64` and `MC30` prescaling, as well as the estimated number of entries from the analysis, the actual number in the factors, the number of delayed pivots, and the backward error, for different finite element types over a mesh of $8 \times 8 \times 2$ finite elements are presented in Table 7.1 and the results over a $16 \times 16 \times 2$ mesh of finite elements in Table 7.2.

We can conclude from the results shown in Tables 7.1 and 7.2 that, for all finite element configurations that we consider, the combination `MA57+MC64` is one order of magnitude faster than `MA57+MC30`. In addition, we found that `MA57` alone, that is without scaling, fails for some configurations because of excessive memory requirements.

The comparison of execution times of `MA57` with the execution times obtained by our formerly used in-house solution code based on a simple band-matrix based sparse Gaussian elimination procedure, is given in Figure 6.2. The finite element configuration HC8/9 is considered because it has the smallest number of entries per row of any other presently considered finite element configuration. The finite element meshes considered are $4 \times 4 \times 2$, $8 \times 8 \times 2$ and $16 \times 16 \times 2$, with 684, 2604 and 10188 degrees of freedom, respectively. We can see that `MA57+MC64` is much faster than the formerly used in-house procedure. If we consider an order of magnitude as an approximate position on a logarithmic scale, the execution time of procedures `MA57+MC30` and `MA57+MC64` in relation to the in-house code, are shown in Figure 6.3.

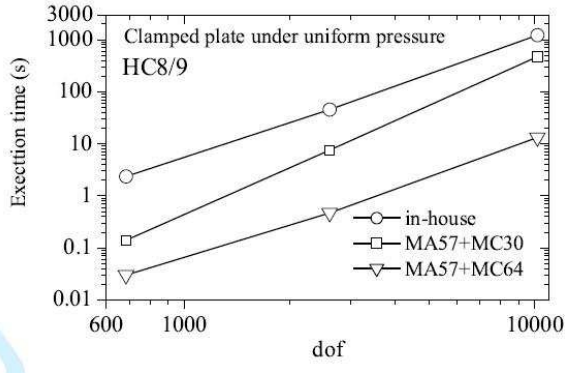

FIGURE 6.2. Clamped Plate – execution time per number of degrees of freedom

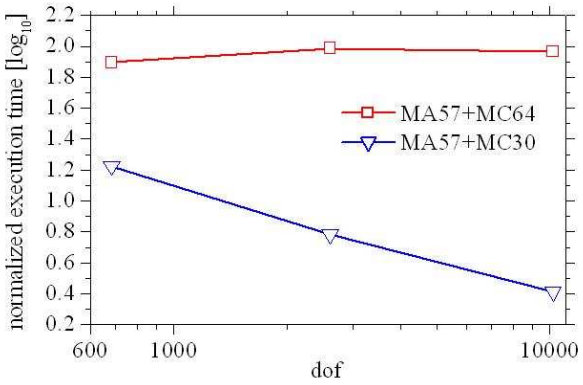

FIGURE 6.3. Clamped Plate – Normalized execution time per number of degrees of freedom

From Figure 6.3 we can see that `MA57+MC64` is about two orders of magnitude faster, while `MA57+MC30` is up to one order of magnitude faster than the previously used simple Gaussian elimination procedure. This time ratio is even bigger for the richer FE

configurations. Therefore, we can say that the use of *HSL* `MA57` solution routines actually enables investigation of richer finite element configurations on personal computers.

6.2. **Long steel coated shaft loaded by the uniform traction.** The second example is from the class of geometrically multiscale model problems. It is a thermal barrier coated component, that is a long hollow shaft coated by a microsized coating [38]. The coating consists of a bond and ceramic layer of equal size. The simulation of the coated materials is of particular interest to industry, due to the need to control the level of the interfacial stresses on the surfaces of material discontinuities. Hexahedral finite elements will differ in size up to four orders of magnitude, which is impossible to solve by a standard primal finite element scheme due to stability problems [1]. The inner and outer radii of the shaft are $0.005\,m$ and $0.1\,m$, respectively. The structural reference temperature is $T_{\text{ref}} = 1000\,^{\circ}\text{C}$. The thickness of the coating (bond and ceramic) is $t = 10^{-5}m$. The height of the shaft is assumed to be $h = 0.1\,m$. Uniform traction $p = -1000MPa$ is prescribed on the outer boundary. This tends to separate the coating from the blade surface. The material properties are given in Table 7.3.

The behaviour of the current finite element scheme with a two dimensional conventional boundary-element approach (CBEM [38]) was compared in [15]. It was shown that, as the coating thickness decreases, the solution remains stable and accurate. Therefore, we will now investigate the execution time that was not investigated before. The target solution is obtained by plain strain theory, that is, theory based on dimensional reduction. A similar problem can be found in the analysis of thin discontinuity layers in solids, such as in the case of fractures in concrete, rock or geomaterials, or of shock waves in compressible fluids [40].

It was proved in [13] that the current finite element approach is reliable with respect to the aspect ratio of its dimensions. Therefore, only one finite element layer is used along the thickness. Both bond and ceramic regions are discretized by three finite element layers along the radius. Due to the symmetry, only one-quarter of the model problem is analyzed. We investigate the execution time for the finite element configurations HC8/9, HC8/27, HC20/21 and HC20/27. Consequently, the maximum finite element aspect ratio is equal to 60000, as shown in Figure 6.4 .

Execution times for three distinct phases in the solution process and storage requirements for `MA57`, with and without scaling (`MC30` and `MC64`), are reported in Table 7.4. It can be seen from this table that scaling the system matrix using `MC30` or `MC64` routines prior to the factorization considerably improves the execution time. In addition, if scaling is used, the storage requirements and number of operations are far smaller. Scaling thus enables the solution of systems with many more degrees of freedom [23]. We can also see that `MA57` without scaling is not able to solve equations using the stable finite element HC8/27 in geometrically multiscale model problems because the factorization fails because of excessive memory requirements. Therefore, the first conclusion is that scaling generally decreases the storage requirements, and that the storage requirement is less for the `MC64` type of scaling. We also note that the factorization times using `MC30` are faster than those using `MC64` but, on further investigation, we found that the `MC64` scaling produces better factors and the time is only higher because of the time taken by `MC64` itself. In fact

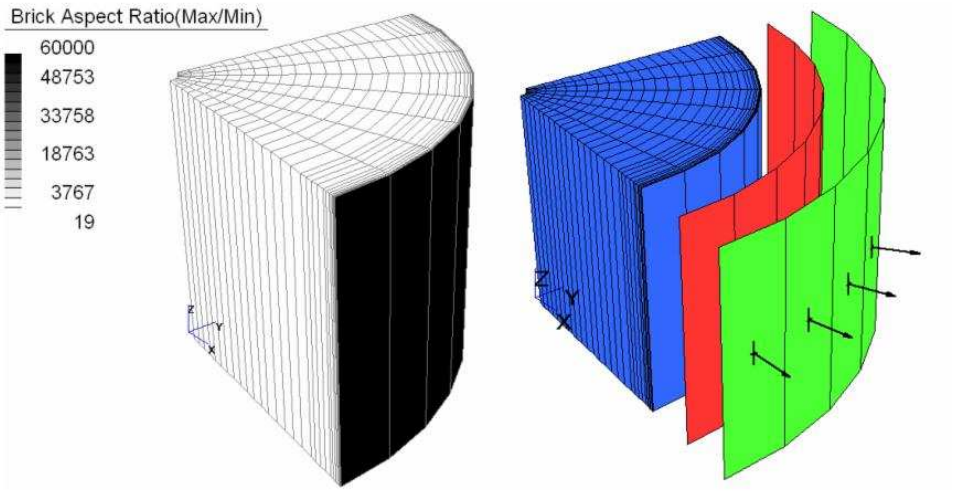

FIGURE 6.4. Coated shaft – finite element mesh aspect ratio and layerwise view

these problems all have very fast factorize times and, because `MC64` has lower complexity than the numerical factorization, the extra time will not be dominant when solving larger problems. We show a sequence of larger problems in Table 7.5, which have been obtained from the HC8/9 finite elements in Table 7.4 by using an increasing number of elements in the z-direction (there was only one element in the Table 7.4 runs and we use 2, 4, 8, 10, 13, and 16 in the six examples in Table 7.5). From the results presented above we see that, on the larger problems, the scaling time for `MC64` is less important. In addition, while the storage requirements for the factorization after scaling by `MC64` are almost the same as in the analysis, the factorization after the `MC30` scaling generates far denser factors, increasingly so as the problem size increases. As an interesting aside to this set of problems, the given matrix has many entries of very small size (around 10^{-20}). However, these are significant numbers inasmuch if they are treated as zero, it is not possible to solve the resulting systems because the matrix is singular.

6.3. **Long steel coated shaft loaded by the prescribed temperature.** In the previous example, the loading was mechanical. We now examine the case where the long coated shaft is loaded by prescribed temperatures on the inner and outer surfaces, such that $T_i = 773^0C$ and $T_o = 1273^0C$, respectively [38]. Therefore, the stresses due to thermal mismatch will be developed in thin coatings. Thermal stress can be significant when a large difference in physical and thermal properties of the bonded materials exists [41]. Note that the system matrix will be unchanged and in this particular case the different loading only modifies the right-hand side in our formulation. Thermal stresses on the surfaces of material discontinuities were sought and the results were reported in [15]. As the matrices are identical, the data on factorization is as is given in Table 7.4. The backward errors in this case were marginally worse but all in the range .7 10^{-9} to .2 10^{-7}.

The target solution of radial stress is obtained by modified plate theory. We will investigate the convergence of the temperature and radial stress component on the interface $L2$, between bond and ceramics, for the sequence of five model problems with decreasing coating thickness $h = 10^{-N}$, where $N = 2, 3, 4, 5, 6$. Consequently, for the last model

problem, where the coating has thickness of $h = 10^{-6}$, we will have the maximum finite element aspect ratio equal to 600000. The temperature and heat flux, and thermal stress results at interface $L2$ obtained by the finite element HC8/9, HC8/27 and a classical plane boundary-element method (CBEM) [39] as the thickness of coating decreases, are shown in Figures 6.5 and 6.6, respectively.

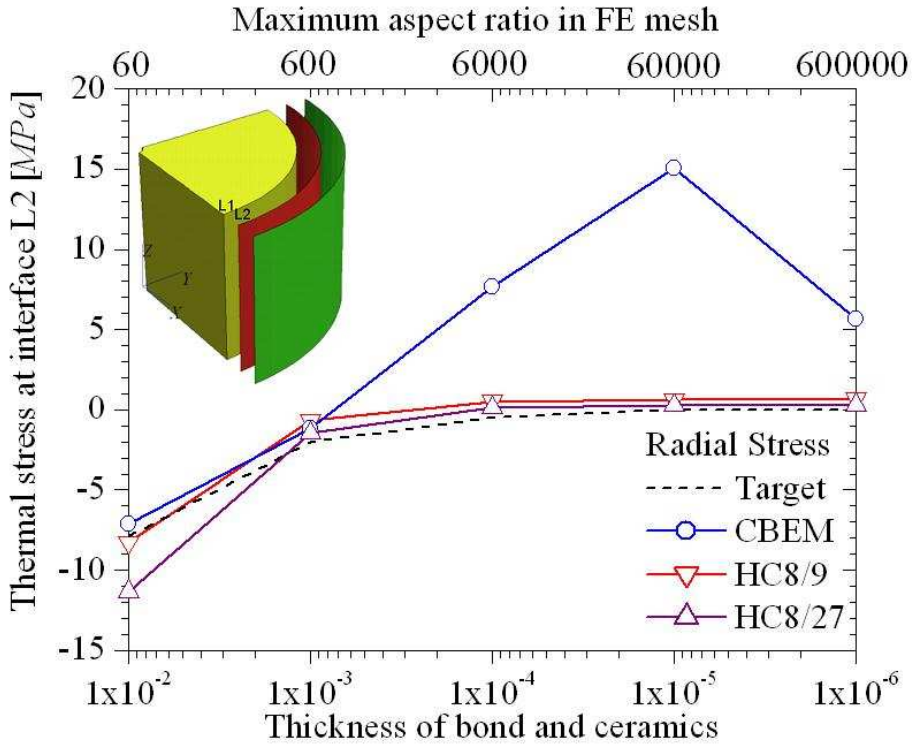

FIGURE 6.5. Coated shaft – Temperature and heat flux interface $L2$ for decreasing thickness of coating

6.4. **Nanoindentation. One–to–one bridging with molecular dynamic simulation.** Bridging over the scales generates perennial interest in the research community since it offers the advantage of combining a deeper understanding of the underlying physical phenomena facilitated by particle mechanics (e.g. for example molecular dynamics – MD), with the computational expediency of continuum mechanics (e.g. finite element method – FE) [7].

In the present example, we study the time and storage efficiency of our current primal–mixed finite-element approach HC$\mathbf{u/t}$ in computational modelling ranging from the continuum up to submicronic scales. Direct kinematic coupling (one–to–one bridging) is performed on the interface surface between two domains. Namely, the displacements of the boundary atoms of the MD domain are introduced as essential boundary conditions to the boundary nodes of the continuum finite-element domain (CM), and vice versa, until equilibrium is reached. Let us note that a direct linking scheme should be the most reliable and desirable boundary condition [18] as it is both numerically robust and efficient. Let us emphasize that the molecular dynamic simulation that we presently consider is based on

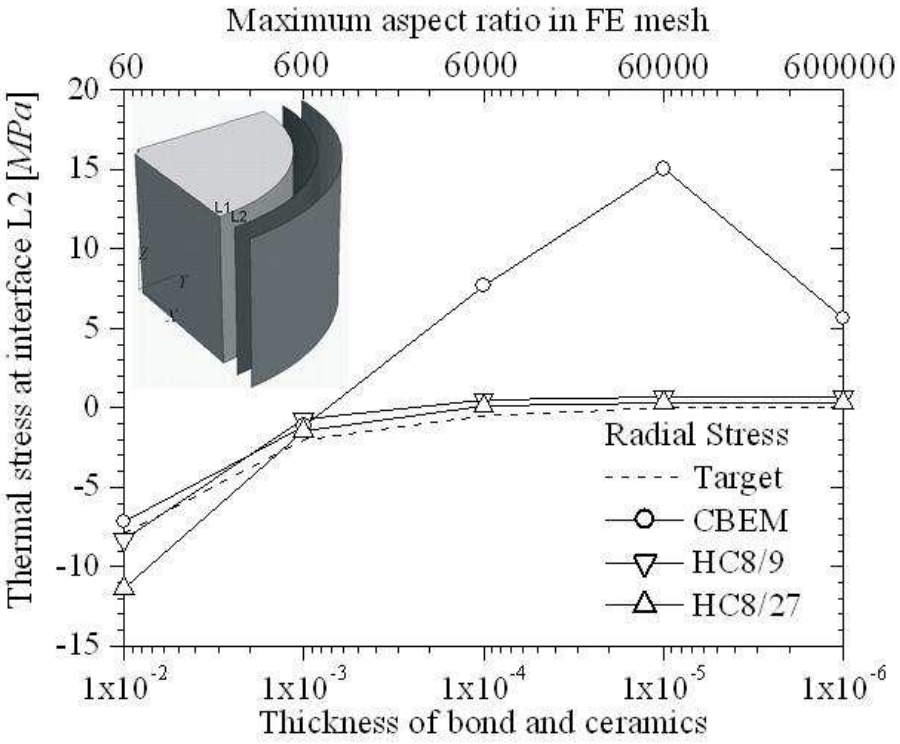

FIGURE 6.6. Coated shaft – Thermal stress at interface $L2$ for decreasing thickness of coating

conventional molecular dynamics using an embedded atom interatomic potential, so the momentum transfer is conserved.

It should be emphasized that in the present example we exploit the reliability (accuracy and stability) of the primal–mixed finite element HC8/27 in a geometrically multiscale simulation [16], where the aspect ratio of FE is up to 7 orders of magnitude, and the geometrical scale resolutions of the model problem is up to 8 orders of magnitude, for both compressible and nearly incompressible materials.

As an numerical example, we consider an atomically sharp rigid indenter that comes into contact with an ideally flat substrate [19]. The substrate material is considered to be titanium with Young's modulus $E = 116\ GPa$ and Poisson's ratio $\nu = 0.36$, and an ultimate tensile strength of 1380 MPa. The dimensions of the whole model problem are $2.02 \cdot 10^{-4}m \times 1.01 \cdot 10^{-4}m$. A domain of the molecular domain patch directly under the nanoindenter is $1.16 \cdot 10^{-9}m \times 1.507 \cdot 10^{-8}m$. The rest of the domain is simulated by the present approach and finite element HC8/9 [19]. One of three consecutively refined HC8/9 finite-element meshes of the continuum domain, and an embedded MD domain patch are shown in Figure 6.7.

From the visualization of the displacement component u_y shown in Figure 6.8, we can see that there are no spurious oscillations of the results [7].

We can see from the time and storage efficiency results shown in Table 7.6 that the combination `MA57+MC64` is superior to the combination `MA57+MC30` in the solution of the resulting large system of linear equations, as we might expect from our earlier experience.

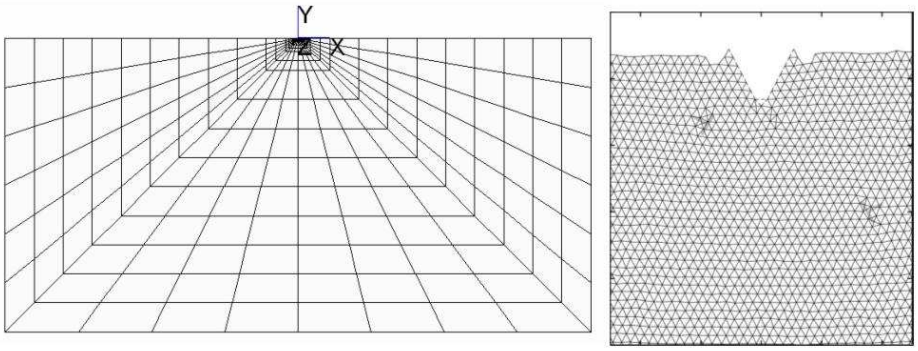

FIGURE 6.7. Nanoindentation model problem

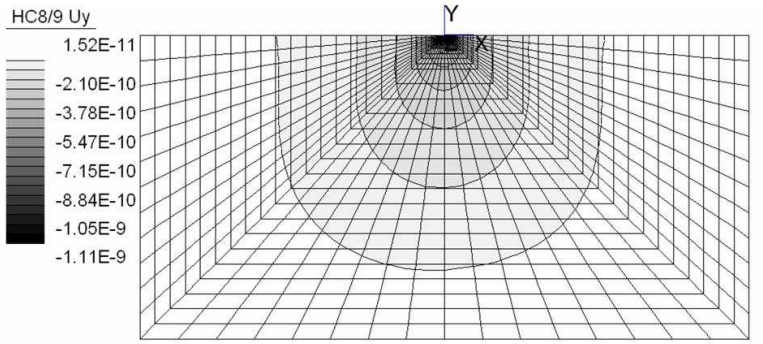

FIGURE 6.8. Nanoindentation model problem: u_y displacement field after first iteration

It should be noted that future work will be oriented towards the introduction of minimal kinematic boundary conditions [42] between the two domains, especially in cases when the MD domain is larger than at present.

6.5. **Composite material with embedded fibre optic sensor.** We now study a laminar composite material under static indentation loading [43]. The composite material is a laminar plate $142 \times 157 \times 7.3\ mm$ in size which consists of 26 aramid fabric layers within the PVB matrix, with an embedded fibre optic sensor between first and second lamina. The optical fibre is simulated with all its three component layers: optic core, optic cladding and optic coating (see Figure 6.9). The material properties of the component materials are given in Tables 7.7 and 7.8. Only one fourth of the model problem is analysed due to the symmetry. The finite element mesh has 4797 finite elements. We can see that considered FE mesh of the optical fibre is not uniform and it is rather coarse, exploiting the reliability of present finite element in geometrically multiscale analysis [16].

The experimental testing was performed ten times. The test specimens are loaded by a force of $F = 15\ kN$ over the circular area with radius of $r = 3.34\ mm$ [43]. The mean value of the measured deflections under the indenter was found to be $u_z = 1.1\ mm$. We can see in Figure 6.10 that the maximal displacement obtained by the present approach is in high agreement with the available experimental data.

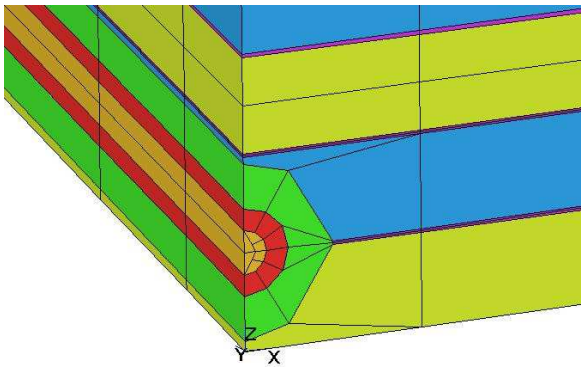

FIGURE 6.9. The part of the composite material finite element model problem. Aramid plies: dark and bright grey. Thin bond layers between the plies which simulates extras PVB between kevlar fabric: very dark grey. Optical fibre: bright grey is optical core, very dark grey is optical cladding, and gray is optical coating.

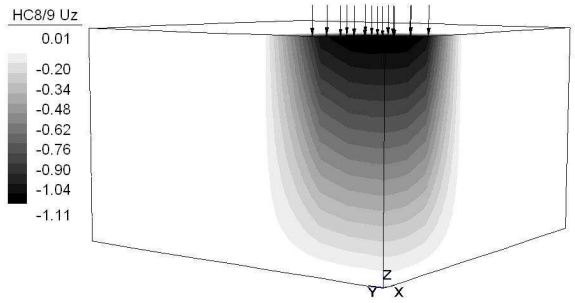

FIGURE 6.10. Composite material: The displacement field u_z obtained by the finite element HC8/9.

The stress field t^{xx} is visualized in Figure 6.11. We can see that there is no spurious oscillation of stresses. Furthermore, the expected different levels of stress in the PVB are also captured. In addition the stress field of the fibre can be clearly distinguished from the surrounding area.

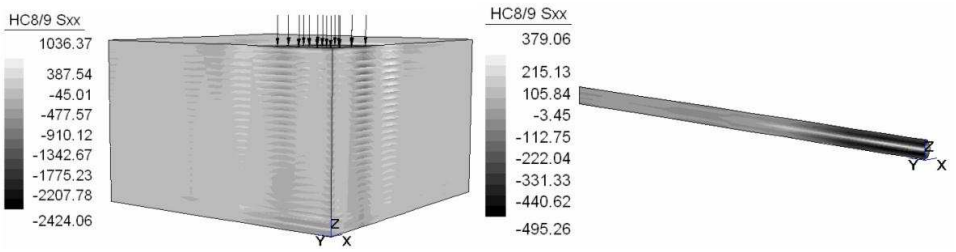

FIGURE 6.11. Composite material: The stress component t^{xx} obtained by the finite element HC8/9, whole model and optical fibre only (all three layers).

The execution time and storage for the combination HC8/9+`MA57`+`MC64`, for three consecutively refined finite element meshes are given in Table 7.9. Let us not that the backward error is for all three examples less than $1 \cdot 10^{-9}$.

7. Conclusion

We have demonstrated the accuracy and time execution efficiency of a fully three-dimensional coordinate independent multifield finite-element approach for the simulation of geometrically multiscale isotropic, orthotropic, nearly incompressible and multi-material solid bodies, based on Hellinger-Reissner's principle with no dimensional reduction and C^0 continuous discretization of the displacement and stress fields. The essential contribution of the present approach in solid mechanics is that it enables the introduction of the residual stresses and initial (thermal or mechanical) strains directly, without differentiation and without consistency error. In addition, it is invariant to mesh distortion or high aspect ratio of the finite elements, and thus is an ideal candidate for bridging with simulations at a particle level, which we have demonstrated by the example of nanoindentation of an titanium alloy. The invariance to the aspect ratio of the finite elements is also used to simulate thin aramid composite materials with embedded optic fibres avoiding any dimensional reduction and with minimum simplification in material composition.

It should be noted that stresses and displacements are simultaneously calculated which leads to the solution of large scale indefinite systems of finite element equations. The equation system is extremely poorly scaled in geometrically multiscale analysis, and it is usually not possible to solve this without special matrix scaling techniques. After detailed investigation we have found that the *HSL* direct sparse solver `MA57` and the system matrix scaling routine `MC64` enables the solution of the assembled equation system by using the current formulation in multiscale analysis.

The first conclusion is that the scaling routine `MC64` substantially decreases the storage requirements and thus enables the solution of larger and more complex systems without upgrading the computing platform. We also performed some runs with the HSL scaling routines `MC30` and `MC77`. We do not report the `MC77` scaling routine runs here as they were always inferior to the `MC64` results although sometimes marginally so. If the model problem is geometrically multiscale the scaling routine `MC30` is competitive although it will only be faster on small problems because, on larger problems, the reduction in the factorization time will more than outweigh the extra cost of implementing the `MC64` scaling. The second conclusion is that the use of any of the scaling routines significantly increases the accuracy of the solution obtained using the `MA57` code. In addition, it is found that the present solution approach is almost three orders of magnitude faster than a formerly used in–house solution approach (see Tables 4 and 6).

Consequently, the satisfaction of the convergence requirements of the present finite element scheme makes it a promising field for future research, including developments for the analysis of materially nonlinear solid continua, or for coupling with other physical fields, such as fluid or electro-magnetic.

Acknowledgements

We would like to thank Scott Sloan of the University of Newcastle, NSW, for looking at the manuscript and making some helpful suggestions. In addition we would like to thank Sreten Mastilovic for providing us results of molecular dynamic simulations that were bridged with the present approach. The work of the first author was supported by

the EPSRC grants EP/E053351/1 and EP/F006535/1. The work of the second author was supported by the Ministry of Science of Republic of Serbia grant 144007.

References

1. Arnold DN. Mixed finite element methods for elliptic problems. *Computer Methods in Applied Mechanics and Engineering* 1990; **82**:281–300
2. Rannacher R, Suttmeier FT. A feed-back approach to error control in finite element methods: application to linear elasticity, *Computational Mechanics* 1997; **19**(5):434–446
3. Brezzi F, Bathe KJ. A Discourse on the Stability Conditions for Mixed Finite Element Formulations, *Journal of Computer Methods in Applied Mechanics and Engineering* 1990; **82**:27–57
4. Bathe KJ, The Inf-Sup Condition and its Evaluation for Mixed Finite Element Methods, *Computers & Structures* 2001; **79**:243–252
5. Bathe KJ. *Finite element procedures*. Englewood Cliffs, NJ: Prentice Hall; 1996.
6. Kim DN, Bathe KJ. A 4-node 3D-shell element to model shell surface tractions and incompressible behavior. *Computers & Structures* 2008; **86**:2027–2041
7. Belytschko T, Xiao SP. Coupling methods for continuum model with molecular model. *International Journal for Multiscale Computational Engineering* 2003; **1**(1): 115–126. DOI: 10.1615/IntJMultCompEng.v1.i1.100
8. Schmauder S, Weber U, Soppa E. Computational mechanics of heterogeneous materials–influence of residual stresses. *Computational Materials Science* 2003; **26**: 142–153, DOI: 10.1016/S0927-0256(02)00414-7
9. Babuska I, Vogelius M. On a dimensional reduction method. III, A-posteriori error estimation and an adaptive approach. *Mathematics of Computation* 1981; **37**:156,361–383, DOI: 10.2307/2007498
10. Shepherd MS. Finite element modelling within an integrated geometric modelling environment: Part II Attribute specification, domain differences and indirect element types. *Engineering with Computers* 1985; **1**:61–71, DOI: 10.1007/BF01200065
11. Oden JT, Brauchli HJ. On the calculation of consistent stress distributions in finite element approximations. *International Journal for Numerical Methods in Engineering* 1971; **3**:317–325
12. Mijuca D, Draskovic Z, Berkovic M. *Displacement based stress recovery procedure*. Advances in Finite Element Technology, Civil-Comp Press, 1996; 127–134
13. Mijuca D. On hexahedral finite element HC8/27 in elasticity. *Computational Mechanics* 2004; **33**(6): 466–480, DOI 10.1007/s00466–003–0546–9
14. Mijuca D, Ziberna A, Medjo B. A new multifield finite element method in steady state heat analysis. *Thermal Science* 2005; **9**(1):111–130
15. Mijuca D, Ziberna A, Medjo B. A novel primal–mixed finite element approach for heat transfer in solids. *Computational Mechanics* 2007; **39**(4): 367-381; DOI: 10.1007/s00466-006-0034-0
16. Mijuca D. On a reliable finite element approach in multiscale multimaterial solid thermo– mechanics, *Journal of the Serbian Society for Computational Mechanics* 2008; **2**(1):44–62
17. Brezzi F, Fortin M, Marini D. Mixed finite element methods with continuous stresses. *Mathematical Models and Methods in Applied Sciences* 1993; **3**(2):275–28
18. Ghoniem NM, Esteban PB, Busso EP, Kioussis N, Huang H. Multiscale modelling of nanomechanics and micromechanics: an overview. *Philosophical Magazine* 2003; **83**(31):3475–3528, DOI: 10.1080/14786430310001607388
19. Mijuca D, Mastilovic S. A novel one-to-one multiscale approach to computational mechanics of materials. 1st International Workshop on Nanoscience and Nanotechnology. IWON 2005 and 4th COSENT Annual Meeting Belgrade, 2005, November 15–18: 180–186
20. Mijuca D, Berkovic M. On the main properties of the primal-mixed finite element formulation. *Facta Universitatis Series Mechanics, Automatic Control And Robotics* 1999; **2**(9):903–920
21. Duff IS, Reid JK. MA47, a Fortran code for direct solution of indefinite sparse symmetric linear systems. *Technical Report RAL–95–001*, Rutherford Appleton Laboratory, Oxfordshire, UK, 1995.

22. Duff IS. MA57 – A code for the solution of sparse symmetric indefinite systems. *ACM Transactions on Mathematical Software* 2004; **30**(2): 118–144, DOI: 10.1145/992200.992202
23. Duff IS, Pralet S. Strategies for scaling and pivoting for sparse symmetric indefinite problems. *SIAM Journal on Matrix Analysis and Applications* 2005; **27**(2):313–340, DOI: 10.1137/04061043X
24. Cannarozzi AA, Ubertini F. A mixed variational method for linear coupled thermoelastic analysis. International *Journal of Solids and Structures* 2001; **38**(4):717-739, DOI: 10.1016/S0020-7683(00)00061-5
25. Green AE, Lindsay KE. Thermoelasticity. *Journal of Elasticity* 1972; **2**(1):1–7
26. Benzi M, Golub GH, Liesen J. Numerical Solution of Saddle Point Problems. *Acta Numerica*, Cambridge University Press. 2005; **14**:1–137, DOI: 10.1017/S0962492904000212
27. Duff IS, Erisman AM, Reid JK. *Direct Methods for Sparse Matrices*. Oxford University Press, London, 1986
28. GStraus7, G+D Computing. *Finite element analysis system software package – Verification Manual*, www.strand.aust.com, Australia
29. HSL (2007) HSL 2007: A collection of Fortran codes for large scale scientific computation, `http://www.cse.scitech.ac.uk/nag/hsl/hsl.shtml`
30. Gould NIM, Scott JA. A numerical evaluation of HSL packages for the direct solutions of large sparse, symmetric linear systems of equations. *Technical Report RAL–TR–2003–019*, Rutherford Appleton Laboratory, Oxfordshire, UK, 2003.
31. Reid JK, Curtis AR. On the automatic scaling of matrices for Gaussian elimination. *J Inst Maths Applics*. 1972; **10**(1): 118–124, DOI: 10.1093/imamat/10.1.118
32. Duff IS, Koster J. On algorithms for permuting large entries to the diagonal of a sparse matrix, *SIAM Journal on Matrix Analysis and Applications*. 2001; **22**(4):973–996, DOI: 10.1137/S0895479899358443
33. Amestoy PR, Davis TA, Duff IS. An approximate minimum degree ordering algorithm. *SIAM Journal on Matrix Analysis and Applications*. 1996; **17**(4):886–905, DOI: 10.1137/S0895479894278952
34. Duff IS, Reid JK. MA27 – A set of Fortran subroutines for solving sparse symmetric sets of linear equations. *AERE R10533*, Her Majesty's Stationery Office, London. 1982.
35. Karypis G, Kumar V MeTiS – A Software Package for Partitioning Unstructured Graphs, Partitioning Meshes, and Computing Fill-Reducing Orderings of Sparse Matrices – Version 4.0. University of Minnesota. 1998.
36. Pellegrini F, Roman J, Amestoy PR. *Hybridizing nested dissection and halo approximate minimum degree for efficient sparse matrix ordering*. In *Proceedings of Irregular'99, San Juan*, Lecture Notes in Computer Science **1586**: 986–995, Springer–Verlag. 1999.
37. Arioli M, Demmel JW, Duff IS. Solving sparse linear systems with sparse backward error. *SIAM Journal on Matrix Analysis and Applications*, 1989; **10**(2):165–190. DOI: 10.1137/0610013
38. Lu S, Dong M. An advanced BEM for thermal and stress analyses of components with thermal barrier coating. *Electronic Journal of Boundary Elements*, 2003; **1**(2):302–315
39. Roark RJ, Young WC. Formulas for Stress and strain. McGraw-Hill. Fifth Edition. 1975
40. Onate E. Multiscale computational analysis in mechanics using finite calculus: an introduction. *Computer Methods in Applied Mechanics and Engineering*. 2003; 192(28-30):3043–3059; DOI: 10.1016/S0045-7825(03)00340-2
41. Haider J, Rahman M, Corcoran B, Hashmi MSJ. Simulation of thermal stress in magnetron sputtered thin coating by finite element analysis. *Journal of Materials Processing Technology* 2005; **168**(1):36–41 DOI: 10.1016/j.jmatprotec.2004.09.093
42. Mesarovic S, Padbidri J. Minimal kinematic boundary conditions for simulations of disordered microstructures. *Philosophical Magazine*, 2005; **85**(1):65–78; DOI: 10.1080/14786430412331313321
43. Zivkovic I, Maksimovic S, Aleksic R. (2004) Numerical and experimental analysis of initial failure of composite laminates with embedded fibreoptic sensors. *Structural Integrity and Life* 2004; **4**(3):137–148

TABLE 7.1. Clamped Plate – elasticity: execution time, storage requirements – number of entries (estimated and actual), number of delayed pivots, backward error, FE mesh $8 \times 8 \times 2$

Clamped plate, finite element mesh $8 \times 8 \times 2$										
FE	N	NE	Time				Number entries ($\times 10^3$)		Nmb. of delayed pivots	Backward error
							Est.	Actual		
			Analyse	Factorize	Solve	Total				
MA57+MC30										
HC8/9	2604	194008	.02	2.98	.03	3.03	458	1494	6863	...5E-11
HC20/21	7380	904759	.16	79.62	.17	79.95	2848	13560	26634	.1E-10
HC8/27	8708	1461997	.14	36.30	.12	36.56	3710	9281	16714	.9E-11
HC20/27	10164	1515891	.23	94.73	.23	95.19	4046	16998	35002	.1E-10
MA57+MC64										
HC8/9	2604	194008	.01	.38	.00	.39	458	458	0	.1E-10
HC20/21	7380	904759	.15	8.60	.07	8.82	2848	5078	10076	.3E-10
HC8/27	8708	1461997	.14	4.77	.04	4.95	3710	3710	0	.2E-10
HC20/27	10164	1515891	.24	10.06	.08	10.38	4046	6627	12135	.3E-10

TABLE 7.2. Clamped Plate – elasticity: execution time, storage requirements, number of delayed pivots, backward error, FE mesh $16 \times 16 \times 2$

Clamped plate, finite element mesh $16 \times 16 \times 2$										
FE	N	NE	Time				Number entries ($\times 10^3$)		Nmb. of delayed pivots	Backward error
							Est.	Actual		
			Analyse	Factorize	Solve	Total				
MA57+MC30										
HC8/9	10188	830584	.08	43.70	.17	43.95	2730	11941	28269	.5E-11
HC20/21	28948	3573009	.34	816.05	2.01	818.40	16941	54287	62265	.6E-11
HC8/27	33908	6102829	.61	996.48	1.63	998.72	26003	82894	77289	.1E-10
HC20/27	39892	6102829	1.64	1629.47	2.37	1633.48	26009	82900	83272	.1E-10
MA57+MC64										
HC8/9	10188	830584	.08	2.62	.05	2.75	2730	2730	0	.2E-10
HC20/21	28948	3573009	.95	108.39	.64	109.98	16941	16941	5983	.2E-10
HC8/27	33908	6102829	.61	65.03	.36	66.00	26003	26003	0	.3E-10
HC20/27	39892	6102829	.59	67.10	.37	68.06	26009	26009	5983	.3E-10

TABLE 7.3. Long steel coated shaft – material properties

Region	Material	Elastic Modulus $E[MPa]$ ($\times 10^4$)	Poisson's ratio ν	Thermal expansion coefficient $\alpha[^\circ\mathrm{C}^{-1}]$ ($\times 10^{-5}$)	Density $\rho[kg]$ ($\times 10^3$)	Thermal conductivity $k[W/m\,^\circ\mathrm{C}]$
Ω_1	Ceramic	1.0	0.25	1.0	4.0	1
Ω_2	Bond	13.7	0.27	1.51	4.0	25
Ω_3	Steel	21.0	0.30	2.0	7.98	25

TABLE 7.4. Long steel coated shaft – execution time and storage requirements

Clamped plate, finite element mesh $8 \times 8 \times 2$										
FE	N	NE	Time				Number entries ($\times 10^3$)		Nmb. of delayed pivots	Backward error
							Est.	Actual		
			Analyse	Factorize	Solve	Total				
In – house, simple Gaussian elimination										
HC8/9	5776			14.31	.75	15.06				
HC20/21	16500			1810.17	4.89	1815.06				
MA57										
HC8/9	5776	280056	.03	8.82	.06	8.91	62	3550	32753	...8E-01
HC20/21	16500	1829790	.16	89.23	.23	89.62	4651	17076	44411	.2E-01
HC8/27										fails
HC20/27										fails
MA57+MC30										
HC8/9	5776	280056	.02	.33	.00	.35	705	813	1736	.7E-11
HC20/21	16500	1829790	.17	3.91	.06	4.14	4651	4768	1012	...9E-11
HC8/27	18634	1961070	.19	3.17	.05	3.41	4306	4306	6	...3E-10
HC20/27	22122	2785700	.28	6.82	.08	7.18	6932	7043	846	...8E-11
MA57+MC64										
HC8/9	5776	280056	.03	.50	.01	.54	705	709	71	.8E-12
HC20/21	16500	1829790	.17	12.28	.05	12.50	4651	4782	1106	.1E-10
HC8/27	18634	1961070	.19	4.05	.06	4.30	4306	4306	0	...2E-10
HC20/27	22122	2785700	.27	11.59	.08	11.94	6932	6987	368	.3E-10

TABLE 7.5. Coated cylindrical shaft refined through longitudinal axis – elasticity: execution time, storage requirements, number of delayed pivots, backward error, using finite elements of type HC8/9

Coated cylindrical shaft refined through longitudinal axis, finite element mesh HC8/9										
Num. of Finite Elements	N	NE	Time				Number entries ($\times 10^3$)		Nmb. of delayed pivots	Backward error
							Est.	Actual		
			Analyse	Factorize	Solve	Total				
MA57+MC30										
3440	55840	5026524	Insufficient storage							
4472	71932	6549189	Insufficient storage							
5504	88024	8071854	Insufficient storage							
MA57+MC64										
688	12928	966084	.28	7.08	.09	7.45	2585	2600	153	.4E-07
1376	23656	1981194	.93	34.36	.26	35.55	7428	7436	42	.2E-06
2752	45112	4011414	1.20	226.39	.94	228.53	27996	27996	0	.5E-06
5504	88024	8071854	2.42	1223.09	3.05	1228.56	87358	87358	0	.5E-06
MA57+MC30 on a Dell Dimension 2350 PC at RAL										
688	12928	966084	.85	12.83	.06	13.74	2514	7681	26745	.55D-11
1376	23656	1981194	1.90	79.81	.21	81.92	7133	25600	55493	.18D-11
2752	45112	4011414	4.30	525.07	.73	530.01	20650	89120	125838	.40E-12
3440	55840	5026524	5.40	1164.16	1.06	1170.62	28578	134874	157413	.29D-12
4472	71932	6549189	Insufficient storage							
5504	88024	8071854	Insufficient storage							
MA57+MC64 on a Dell Dimension 2350 PC at RAL										
688	12928	966084	.84	1.61	.02	2.47	2514	2519	46	.85E-12
1376	23656	1981194	1.93	5.66	.06	7.65	7133	7133	0	.97E-12
2752	45112	4011414	4.29	22.06	.16	26.51	20650	20653	7	.11E-11
3440	55840	5026524	5.43	32.80	.23	38.46	28578	28583	7	.12E-11
4472	71932	6549189	7.76	55.76	.32	63.84	40671	40678	17	.89E-12
5504	88024	8071854	9.30	78.48	.43	88.21	54684	54702	30	.12E-11

TABLE 7.6. Nanoindentation – elasticity: execution time, storage requirements, number of delayed pivots, backward error, FE meshes HC8/9

Nanoindentation, finite element mesh HC8/9										
Num. of Finite Elements	N	NE	Time				Number entries ($\times 10^3$)		Nmb. of delayed pivots	Backward error
							Est.	Actual		
			Analyse	Factorize	Solve	Total				
Simple Gaussian Elimination										
508	8588					34527.85				
2032	33432		Insufficient storage							
4572	74612		Insufficient storage							
MA57+MC30										
508	8588	439318	.04	3.25	.03	3.32	1546	3427	13070	.178D-12
2032	33432	1749188	.21	57.04	.21	57.46	7867	25218	60509	.180E-12
4572	74612	3934554	3.95	258.83	.51	263.29	18568	65122	134805	.413D-12
MA57+MC64										
508	8588	439318	.05	1.42	.01	1.48	1546	1549	35	.142D-18
2032	33432	1749188	.22	8.86	.07	9.15	7867	7900	310	.274D-18
4572	74612	3934554	3.99	22.35	.16	26.50	18568	18647	957	.449E-18

TABLE 7.7. Material properties of the optical fibre and PVB

	Young modulus [MPa]	Poisson's ratio
Optic core	82600.0	0.17
Optic cladding	67500.0	0.19
Optic coating	1500.0	0.4
PVB	20000.0	0.4

TABLE 7.8. Material properties of the transversally isotropic aramid material

Material properties of the aramid layers in composite material			
Young modulus [MPa]	$E_{11} = 140000$	$E_{22} = 140000$	$E_{33} = 2700$
Shear Modulus [MPa]	$G_{12} = 920$	$G_{23} = 200$	$G_{13} = 200$
Poisson's ratio	$\nu_{12} = 0.35$	$\nu_{23} = 0.1$	$\nu_{13} = 0.1$

TABLE 7.9. Composite – elasticity: execution time, storage requirements, number of delayed pivots, backward error, FE meshes HC8/9

Composite material with embedded optical fibre, finite element mesh HC8/9										
Num. of Finite Elements	N	NE	Time				Number entries ($\times 10^3$)		Nmb. of delayed pivots	Backward error
							Est.	Actual		
			Analyse	Factorize	Solve	Total				
MA57+MC64										
2172	37339	3247757	.32	34.90	.20	35.42	17408	17426	109	.1E-10
2933	49530	4407126	.56	82.73	.39	83.68	28418	28478	285	.7E-10
4797	79078	7255406	.78	270.30	0.84	271.92	63004	63180	646	.4E-10